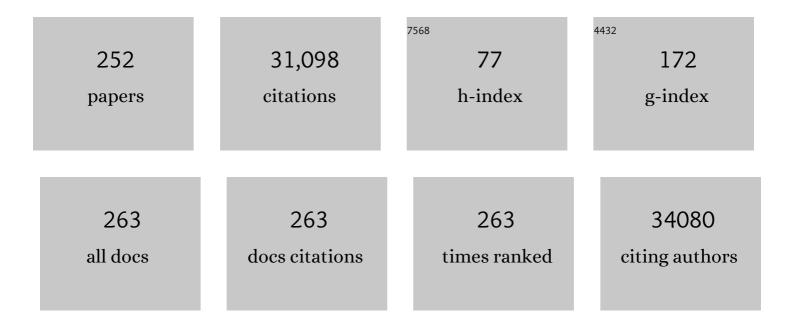
## Takeshi Fujita

List of Publications by Year in descending order

Source: https://exaly.com/author-pdf/3505290/publications.pdf Version: 2024-02-01



Τλέρομι Ειμιτλ

#	Article	IF	CITATIONS
1	Charge partitioning by intertwined metal-oxide nano-architectural networks for the photocatalytic dry reforming of methane. Chem Catalysis, 2022, 2, 321-329.	6.1	9
2	Gasâ€₽hase Photoelectrocatalysis Mediated by Oxygen Ions for Uphill Conversion of Greenhouse Gases. ChemPhotoChem, 2021, 5, 275-281.	3.0	7
3	Tailored Catalytic Nanoframes from Metal–Organic Frameworks by Anisotropic Surface Modification and Etching for the Hydrogen Evolution Reaction. Angewandte Chemie - International Edition, 2021, 60, 4747-4755.	13.8	92
4	Tailored Catalytic Nanoframes from Metal–Organic Frameworks by Anisotropic Surface Modification and Etching for the Hydrogen Evolution Reaction. Angewandte Chemie, 2021, 133, 4797-4805.	2.0	18
5	Terahertz and infrared response assisted by heat localization in nanoporous graphene. Carbon, 2021, 173, 403-409.	10.3	5
6	Nanoporous ultra-high-entropy alloys containing fourteen elements for water splitting electrocatalysis. Chemical Science, 2021, 12, 11306-11315.	7.4	88
7	Active site separation of photocatalytic steam reforming of methane using a gas-phase photoelectrochemical system. Chemical Communications, 2021, 57, 8007-8010.	4.1	7
8	Anomalous enhancement of thermoelectric power factor by thermal management with resonant level effect. Journal of Materials Chemistry A, 2021, 9, 4851-4857.	10.3	20
9	Graphene-coated nanoporous nickel towards a metal-catalyzed oxygen evolution reaction. Nanoscale, 2021, 13, 10916-10924.	5.6	13
10	Distorted planar defects stabilize tetragonal boron. Scripta Materialia, 2021, 194, 113685.	5.2	1
11	Fast attenuation of high-frequency acoustic waves in bicontinuous nanoporous gold. Applied Physics Letters, 2021, 119, .	3.3	2
12	Response to the commentary by Robert Tournier and Michael Ojovan on our publication entitled "Improving glass forming ability of off-eutectic metallic glass formers by manipulating primary crystallization reactions― Scripta Materialia, 2021, 205, 114035.	5.2	3
13	Crystalline boron monosulfide nanosheets with tunable bandgaps. Journal of Materials Chemistry A, 2021, 9, 24631-24640.	10.3	21
14	Methodology of Thermoelectric Power Factor Enhancement by Nanoscale Thermal Management in Bulk SiGe Composites. ACS Applied Energy Materials, 2020, 3, 1235-1241.	5.1	14
15	Metal Carbide as A Lightâ€Harvesting and Anticoking Catalysis Support for Dry Reforming of Methane. Global Challenges, 2020, 4, 1900067.	3.6	17
16	Highâ€Resolution Electrochemical Mapping of the Hydrogen Evolution Reaction on Transitionâ€Metal Dichalcogenide Nanosheets. Angewandte Chemie, 2020, 132, 3629-3636.	2.0	11
17	Highâ€Resolution Electrochemical Mapping of the Hydrogen Evolution Reaction on Transitionâ€Metal Dichalcogenide Nanosheets. Angewandte Chemie - International Edition, 2020, 59, 3601-3608.	13.8	136
18	Acid Assisted Synthesis of HB Sheets through Exfoliation of MgB <sub>2</sub> Bulk in Organic Media. Chemistry Letters, 2020, 49, 1194-1196.	1.3	17

#	Article	IF	CITATIONS
19	Improving glass forming ability of off-eutectic metallic glass formers by manipulating primary crystallization reactions. Acta Materialia, 2020, 200, 710-719.	7.9	16
20	Bismuth/Porous Graphene Heterostructures for Ultrasensitive Detection of Cd (II). Materials, 2020, 13, 5102.	2.9	5
21	Progress in environmental high-voltage transmission electron microscopy for nanomaterials. Philosophical Transactions Series A, Mathematical, Physical, and Engineering Sciences, 2020, 378, 20190602.	3.4	6
22	Intermetallic Pd <sub>3</sub> <i>X</i> ( <i>X</i> = Ti and Zr) nanocrystals for electro-oxidation of alcohols and formic acid in alkaline and acidic media. Science and Technology of Advanced Materials, 2020, 21, 573-583.	6.1	10
23	Active faceted nanoporous ruthenium for electrocatalytic hydrogen evolution. Journal of Materials Chemistry A, 2020, 8, 19788-19792.	10.3	19
24	NiYAl-Derived Nanoporous Catalysts for Dry Reforming of Methane. Materials, 2020, 13, 2044.	2.9	1
25	Intertwined Nickel and Magnesium Oxide Rival Precious Metals for Catalytic Reforming of Greenhouse Gases. Advanced Sustainable Systems, 2020, 4, 2000041.	5.3	2
26	Visible-light-driven dry reforming of methane using a semiconductor-supported catalyst. Chemical Communications, 2020, 56, 4611-4614.	4.1	46
27	Hydrogen Boride Sheets as Reductants and the Formation of Nanocomposites with Metal Nanoparticles. Chemistry Letters, 2020, 49, 789-793.	1.3	16
28	Photocatalytic uphill conversion of natural gas beyond the limitation of thermal reaction systems. Nature Catalysis, 2020, 3, 148-153.	34.4	194
29	Visible-light-driven photocatalysis via reductant-to-band charge transfer in Cr(III) nanocluster-loaded SrTiO3 system. Applied Catalysis B: Environmental, 2020, 270, 118883.	20.2	16
30	Anomalous Nernst effect in Co <i>x</i> (MgO)1- <i>x</i> granular thin films. Applied Physics Letters, 2020, 116, .	3.3	12
31	Photoinduced hydrogen release from hydrogen boride sheets. Nature Communications, 2019, 10, 4880.	12.8	63
32	Operando Observations of SEI Film Evolution by Massâ€ <b>s</b> ensitive Scanning Transmission Electron Microscopy. Advanced Energy Materials, 2019, 9, 1902675.	19.5	64
33	Diversity of Nanoporous Metals. Metals, 2019, 9, 996.	2.3	1
34	3D bicontinuous nanoporous plasmonic heterostructure for enhanced hydrogen evolution reaction under visible light. Nano Energy, 2019, 58, 552-559.	16.0	29
35	Thermoelectric power factor enhancement based on carrier transport physics in ultimately phonon-controlled Si nanostructures. Materials Today Energy, 2019, 13, 56-63.	4.7	39
36	Photocatalytic Partial Oxidation of Methane on Palladium‣oaded Strontium Tantalate. Solar Rrl, 2019, 3, 1900076.	5.8	15

#	Article	IF	CITATIONS
37	Hierarchical Nanoporous Copper Architectures via 3D Printing Technique for Highly Efficient Catalysts. Small, 2019, 15, e1805432.	10.0	31
38	Temperature-dependent compression behavior of an Al0.5CoCrCuFeNi high-entropy alloy. Materialia, 2019, 5, 100243.	2.7	16
39	Topologically immobilized catalysis centre for long-term stable carbon dioxide reforming of methane. Chemical Science, 2019, 10, 3701-3705.	7.4	27
40	CO2 oxidative coupling of methane using an earth-abundant CaO-based catalyst. Scientific Reports, 2019, 9, 15454.	3.3	14
41	Synergistic photothermal and photochemical partial oxidation of methane over noble metals incorporated in mesoporous silica. Chemical Communications, 2019, 55, 13765-13768.	4.1	19
42	Time-resolved atomic-scale observations of deformation and fracture of nanoporous gold under tension. Acta Materialia, 2019, 165, 99-108.	7.9	39
43	Lithium intercalation into bilayer graphene. Nature Communications, 2019, 10, 275.	12.8	136
44	Operando characterization of cathodic reactions in a liquid-state lithium-oxygen micro-battery by scanning transmission electron microscopy. Scientific Reports, 2018, 8, 3134.	3.3	25
45	Light-promoted conversion of greenhouse gases over plasmonic metal–carbide nanocomposite catalysts. Materials Chemistry Frontiers, 2018, 2, 580-584.	5.9	20
46	Three-dimensional bicontinuous nanoporous materials by vapor phase dealloying. Nature Communications, 2018, 9, 276.	12.8	123
47	Synthesizing 1T–1H Two-Phase Mo <sub>1–<i>x</i></sub> W <sub><i>x</i></sub> S <sub>2</sub> Monolayers by Chemical Vapor Deposition. ACS Nano, 2018, 12, 1571-1579.	14.6	62
48	Bilayered nanoporous graphene/molybdenum oxide for high rate lithium ion batteries. Nano Energy, 2018, 45, 273-279.	16.0	54
49	Three-Dimensional Nanoporous Heterojunction of Monolayer MoS <sub>2</sub> @rGO for Photoenhanced Hydrogen Evolution Reaction. ACS Applied Energy Materials, 2018, 1, 2183-2191.	5.1	27
50	Intercalation pseudocapacitance of amorphous titanium dioxide@nanoporous graphene for high-rate and large-capacity energy storage. Nano Energy, 2018, 49, 354-362.	16.0	74
51	Operando observations of RuO2 catalyzed Li2O2 formation and decomposition in a Li-O2 micro-battery. Nano Energy, 2018, 47, 427-433.	16.0	47
52	Scanning distortion correction in STEM images. Ultramicroscopy, 2018, 184, 274-283.	1.9	23
53	Nanoporous Nickel Composite Catalyst for the Dry Reforming of Methane. ACS Omega, 2018, 3, 16651-16657.	3.5	9
54	Graphene-based quasi-solid-state lithium–oxygen batteries with high energy efficiency and a long cycling lifetime. NPG Asia Materials, 2018, 10, 1037-1045.	7.9	35

#	Article	IF	CITATIONS
55	Distortion of Local Atomic Structures in Amorphous Ge-Sb-Te Phase Change Materials. Physical Review Letters, 2018, 120, 205502.	7.8	35
56	Photo-assisted Dry Reforming of Methane over Strontium Titanate. Chemistry Letters, 2018, 47, 935-937.	1.3	19
57	Synthesis of Metastable Au-Fe Alloy Using Ordered Nanoporous Silica as a Hard Template. Metals, 2018, 8, 17.	2.3	5
58	Formation of various epitaxial nanodots in Si films for thermoelectric materials. Journal of Physics: Conference Series, 2018, 1052, 012135.	0.4	0
59	Heavily Doped and Highly Conductive Hierarchical Nanoporous Graphene for Electrochemical Hydrogen Production. Angewandte Chemie, 2018, 130, 13486-13491.	2.0	10
60	Heavily Doped and Highly Conductive Hierarchical Nanoporous Graphene for Electrochemical Hydrogen Production. Angewandte Chemie - International Edition, 2018, 57, 13302-13307.	13.8	64
61	Deformation behaviour of 18R long-period stacking ordered structure in an Mg-Zn-Y alloy under shock loading. Intermetallics, 2018, 102, 21-25.	3.9	3
62	Nobleâ€Metalâ€Free Metallic Glass as a Highly Active and Stable Bifunctional Electrocatalyst for Water Splitting. Advanced Materials Interfaces, 2017, 4, 1601086.	3.7	60
63	Formation Mechanism of Boron-Based Nanosheet through the Reaction of MgB <sub>2</sub> with Water. Journal of Physical Chemistry C, 2017, 121, 10587-10593.	3.1	53
64	Tunable Nanoporous Metallic Glasses Fabricated by Selective Phase Dissolution and Passivation for Ultrafast Hydrogen Uptake. Chemistry of Materials, 2017, 29, 4478-4483.	6.7	38
65	Full Performance Nanoporous Graphene Based Liâ€O <sub>2</sub> Batteries through Solution Phase Oxygen Reduction and Redoxâ€Additive Mediated Li <sub>2</sub> O <sub>2</sub> Oxidation. Advanced Energy Materials, 2017, 7, 1601933.	19.5	65
66	Structure and mechanical properties of boron-rich boron carbides. Journal of the European Ceramic Society, 2017, 37, 4514-4523.	5.7	89
67	Nanophase-separated Ni <sub>3</sub> Nb as an automobile exhaust catalyst. Chemical Science, 2017, 8, 3374-3378.	7.4	18
68	Hierarchical nanoporous metals as a path toward the ultimate three-dimensional functionality. Science and Technology of Advanced Materials, 2017, 18, 724-740.	6.1	50
69	Engineering the internal surfaces of three-dimensional nanoporous catalysts by surfactant-modified dealloying. Nature Communications, 2017, 8, 1066.	12.8	69
70	Chemical Selectivity at Grain Boundary Dislocations in Monolayer Mo <sub>1–<i>x</i></sub> W <sub><i>x</i></sub> S <sub>2</sub> Transition Metal Dichalcogenides. ACS Applied Materials & Interfaces, 2017, 9, 29438-29444.	8.0	10
71	Formation and Characterization of Hydrogen Boride Sheets Derived from MgB <sub>2</sub> by Cation Exchange. Journal of the American Chemical Society, 2017, 139, 13761-13769.	13.7	157
72	Direct Observations of the Formation and Redoxâ€Mediatorâ€Assisted Decomposition of Li <sub>2</sub> O <sub>2</sub> in a Liquidâ€Cell Li–O <sub>2</sub> Microbattery by Scanning Transmission Electron Microscopy. Advanced Materials, 2017, 29, 1702752.	21.0	41

Τακές μι Γυμιτά

#	Article	IF	CITATIONS
73	Tuning Surface Structure of 3D Nanoporous Gold by Surfactantâ€Free Electrochemical Potential Cycling. Advanced Materials, 2017, 29, 1703601.	21.0	54
74	Two-Dimensional Hallmark of Highly Interconnected Three-Dimensional Nanoporous Graphene. ACS Omega, 2017, 2, 3691-3697.	3.5	32
75	Stability limits and transformation pathways of <i>î±</i> -quartz under high pressure. Physical Review B, 2017, 95, .	3.2	15
76	Thermoelectric properties of epitaxial β-FeSi <sub>2</sub> thin films grown on Si(111) substrates with various film qualities. Japanese Journal of Applied Physics, 2017, 56, 05DC04.	1.5	5
77	Correlation between Local Structure Order and Spatial Heterogeneity in a Metallic Glass. Physical Review Letters, 2017, 119, 215501.	7.8	116
78	Embedded-ZnO Nanowire Structure for High-Performance Transparent Thermoelectric Materials. Journal of Electronic Materials, 2017, 46, 3020-3024.	2.2	20
79	Thermoelectric Properties of Epitaxial β-FeSi2 Thin Films on Si(111) and Approach for Their Enhancement. Journal of Electronic Materials, 2017, 46, 3235-3241.	2.2	15
80	In-Situ TEM Study of a Nanoporous Ni–Co Catalyst Used for the Dry Reforming of Methane. Metals, 2017, 7, 406.	2.3	14
81	Effect of Chemical Doping on Cathodic Performance of Bicontinuous Nanoporous Graphene for Liâ€O <sub>2</sub> Batteries. Advanced Energy Materials, 2016, 6, 1501870.	19.5	132
82	3D Bicontinuous Nanoporous Reduced Graphene Oxide for Highly Sensitive Photodetectors. Advanced Functional Materials, 2016, 26, 1271-1277.	14.9	48
83	Valenceâ€band electronic structure evolution of graphene oxide upon thermal annealing for optoelectronics. Physica Status Solidi (A) Applications and Materials Science, 2016, 213, 2380-2386.	1.8	13
84	Versatile nanoporous bimetallic phosphides towards electrochemical water splitting. Energy and Environmental Science, 2016, 9, 2257-2261.	30.8	535
85	Earthâ€Abundant and Durable Nanoporous Catalyst for Exhaustâ€Gas Conversion. Advanced Functional Materials, 2016, 26, 1609-1616.	14.9	18
86	Electric Properties of Dirac Fermions Captured into 3D Nanoporous Graphene Networks. Advanced Materials, 2016, 28, 10304-10310.	21.0	47
87	Correlation between Chemical Dopants and Topological Defects in Catalytically Active Nanoporous Graphene. Advanced Materials, 2016, 28, 10644-10651.	21.0	110
88	An ultrahigh volumetric capacitance of squeezable three-dimensional bicontinuous nanoporous graphene. Nanoscale, 2016, 8, 18551-18557.	5.6	13
89	Chemical Vapor Deposition of Monolayer Mo1â~'xWxS2 Crystals with Tunable Band Gaps. Scientific Reports, 2016, 6, 21536.	3.3	101
90	Hierarchical nanoporosity enhanced reversible capacity of bicontinuous nanoporous metal based Li-O2 battery. Scientific Reports, 2016, 6, 33466.	3.3	52

#	Article	IF	CITATIONS
91	Unveiling Three-Dimensional Stacking Sequences of 1T Phase MoS <sub>2</sub> Monolayers by Electron Diffraction. ACS Nano, 2016, 10, 10308-10316.	14.6	21
92	Atomic-scale disproportionation in amorphous silicon monoxide. Nature Communications, 2016, 7, 11591.	12.8	138
93	Visualizing Under oordinated Surface Atoms on 3D Nanoporous Gold Catalysts. Advanced Materials, 2016, 28, 1753-1759.	21.0	85
94	Non-aqueous nanoporous gold based supercapacitors with high specific energy. Scripta Materialia, 2016, 116, 76-81.	5.2	22
95	Large-scale growth of sharp gold nano-cones for single-molecule SERS detection. RSC Advances, 2016, 6, 2882-2887.	3.6	36
96	On hip Microâ€Pseudocapacitors for Ultrahigh Energy and Power Delivery. Advanced Science, 2015, 2, 1500067.	11.2	66
97	Nanoporous Metal Papers for Scalable Hierarchical Electrode. Advanced Science, 2015, 2, 1500086.	11.2	26
98	Environment-Sensitive Thermal Coarsening of Nanoporous Gold. Materials Transactions, 2015, 56, 468-472.	1.2	22
99	3D Nanoporous Nitrogenâ€Đoped Graphene with Encapsulated RuO <sub>2</sub> Nanoparticles for Li–O <sub>2</sub> Batteries. Advanced Materials, 2015, 27, 6137-6143.	21.0	195
100	Nanoporous Graphene with Singleâ€Atom Nickel Dopants: An Efficient and Stable Catalyst for Electrochemical Hydrogen Production. Angewandte Chemie - International Edition, 2015, 54, 14031-14035.	13.8	628
101	Multifunctional Porous Graphene for Highâ€Efficiency Steam Generation by Heat Localization. Advanced Materials, 2015, 27, 4302-4307.	21.0	769
102	Extraordinary Supercapacitor Performance of a Multicomponent and Mixedâ€Valence Oxyhydroxide. Angewandte Chemie, 2015, 127, 8218-8222.	2.0	16
103	Extraordinary Supercapacitor Performance of a Multicomponent and Mixedâ€Valence Oxyhydroxide. Angewandte Chemie - International Edition, 2015, 54, 8100-8104.	13.8	50
104	Aligned Nanoporous Pt–Cu Bimetallic Microwires with High Catalytic Activity toward Methanol Electrooxidation. ACS Catalysis, 2015, 5, 3779-3785.	11.2	117
105	Visualization of topological landscape in shear-flow dynamics of amorphous solids. Europhysics Letters, 2015, 110, 38002.	2.0	2
106	Sample size induced brittle-to-ductile transition of single-crystal aluminum nitride. Acta Materialia, 2015, 88, 252-259.	7.9	38
107	Promoted C–C bond cleavage over intermetallic TaPt <sub>3</sub> catalyst toward low-temperature energy extraction from ethanol. Energy and Environmental Science, 2015, 8, 1685-1689.	30.8	43
108	A nanoporous metal recuperated MnO <sub>2</sub> anode for lithium ion batteries. Nanoscale, 2015, 7, 15111-15116.	5.6	58

Τακές μι Γυμιτά

#	Article	IF	CITATIONS
109	High Catalytic Activity of Nitrogen and Sulfur Coâ€Đoped Nanoporous Graphene in the Hydrogen Evolution Reaction. Angewandte Chemie - International Edition, 2015, 54, 2131-2136.	13.8	760
110	Covalent functionalization of monolayered transition metal dichalcogenides by phase engineering. Nature Chemistry, 2015, 7, 45-49.	13.6	637
111	Nanoscale phase separation in a fcc-based CoCrCuFeNiAl0.5 high-entropy alloy. Acta Materialia, 2015, 84, 145-152.	7.9	193
112	Direct Observation of High-Temperature Superconductivity in One-Unit-Cell FeSe Films. Chinese Physics Letters, 2014, 31, 017401.	3.3	222
113	Threeâ€Dimensional Hierarchical Nanoporosity for Ultrahigh Power and Excellent Cyclability of Electrochemical Pseudocapacitors. Advanced Energy Materials, 2014, 4, 1301809.	19.5	27
114	Shear amorphization of boron suboxide. Scripta Materialia, 2014, 76, 9-12.	5.2	47
115	Highâ€Quality Threeâ€Dimensional Nanoporous Graphene. Angewandte Chemie - International Edition, 2014, 53, 4822-4826.	13.8	215
116	Bicontinuous Nanoporous Nâ€doped Graphene for the Oxygen Reduction Reaction. Advanced Materials, 2014, 26, 4145-4150.	21.0	261
117	NbPt <sub>3</sub> Intermetallic Nanoparticles: Highly Stable and COâ€Tolerant Electrocatalyst for Fuel Oxidation. ChemElectroChem, 2014, 1, 728-732.	3.4	31
118	Reduced Graphene Oxide Thin Films as Ultrabarriers for Organic Electronics. Advanced Energy Materials, 2014, 4, 1300986.	19.5	59
119	Large Enhancement of Quantum Dot Fluorescence by Highly Scalable Nanoporous Gold. Advanced Materials, 2014, 26, 1289-1294.	21.0	69
120	Monolayer MoS <sub>2</sub> Films Supported by 3D Nanoporous Metals for Highâ€Efficiency Electrocatalytic Hydrogen Production. Advanced Materials, 2014, 26, 8023-8028.	21.0	299
121	The synergistic effect of nanoporous AuPd alloy catalysts on highly chemoselective 1,4-hydrosilylation of conjugated cyclic enones. Chemical Communications, 2014, 50, 3344.	4.1	31
122	Low-temperature solution-processable Ni(OH) <sub>2</sub> ultrathin nanosheet/N-graphene nanohybrids for high-performance supercapacitor electrodes. Nanoscale, 2014, 6, 5960-5966.	5.6	41
123	Chemically exfoliated ReS <sub>2</sub> nanosheets. Nanoscale, 2014, 6, 12458-12462.	5.6	160
124	Inelastic electron-tunneling spectroscopy of nanoporous gold films. Physical Review B, 2014, 89, .	3.2	4
125	Mixing Time of Molecules Inside of Nanoporous Gold. SIAM Journal on Applied Mathematics, 2014, 74, 1298-1314.	1.8	3
126	Stimulation of Electro-oxidation Catalysis by Bulk-Structural Transformation in Intermetallic ZrPt <sub>3</sub> Nanoparticles. ACS Applied Materials & Interfaces, 2014, 6, 16124-16130.	8.0	35

#	Article	IF	CITATIONS
127	Selfâ€Grown Oxyâ€Hydroxide@ Nanoporous Metal Electrode for Highâ€Performance Supercapacitors. Advanced Materials, 2014, 26, 269-272.	21.0	152
128	Structural origins of Johari-Goldstein relaxation in a metallic glass. Nature Communications, 2014, 5, 3238.	12.8	144
129	Asymmetric twins in rhombohedral boron carbide. Applied Physics Letters, 2014, 104, 021907.	3.3	32
130	Nanoporous metal based flexible asymmetric pseudocapacitors. Journal of Materials Chemistry A, 2014, 2, 10910-10916.	10.3	87
131	Atomic Observation of Catalysis-Induced Nanopore Coarsening of Nanoporous Gold. Nano Letters, 2014, 14, 1172-1177.	9.1	109
132	Fabrication of large-scale nanoporous nickel with a tunable pore size for energy storage. Journal of Power Sources, 2014, 247, 896-905.	7.8	140
133	Structural Study of Zr-Cu-Ag Bulk Metallic Glasses Using the Anomalous X-ray Scattering Method. Journal of Physics: Conference Series, 2014, 502, 012027.	0.4	2
134	Non-invasive measurement of glucose uptake of skeletal muscle tissue models using a glucose nanobiosensor. Biosensors and Bioelectronics, 2013, 50, 194-201.	10.1	20
135	High-energy-density nonaqueous MnO2@nanoporous gold based supercapacitors. Journal of Materials Chemistry A, 2013, 1, 9202.	10.3	84
136	Geometric Frustration of Icosahedron in Metallic Glasses. Science, 2013, 341, 376-379.	12.6	423
137	Conducting MoS <sub>2</sub> Nanosheets as Catalysts for Hydrogen Evolution Reaction. Nano Letters, 2013, 13, 6222-6227.	9.1	1,948
138	A Coreâ€Shell Nanoporous Ptâ€Cu Catalyst with Tunable Composition and High Catalytic Activity. Advanced Functional Materials, 2013, 23, 4156-4162.	14.9	118
139	Atomic structure of amorphous shear bands in boron carbide. Nature Communications, 2013, 4, 2483.	12.8	190
140	Ultrahigh capacitance of nanoporous metal enhanced conductive polymer pseudocapacitors. Journal of Power Sources, 2013, 225, 304-310.	7.8	52
141	Synergistic alloying effect on microstructural evolution and mechanical properties of Cu precipitation-strengthened ferritic alloys. Acta Materialia, 2013, 61, 7726-7740.	7.9	85
142	Unsupported Nanoporous Gold Catalyst for Highly Selective Hydrogenation of Quinolines. Organic Letters, 2013, 15, 1484-1487.	4.6	99
143	Microstructure characterization of Cu-rich nanoprecipitates in a Fe–2.5 Cu–1.5 Mn–4.0 Ni–1.0 Al multicomponent ferritic alloy. Acta Materialia, 2013, 61, 2133-2147.	7.9	153
144	Enhanced Supercapacitor Performance of MnO <sub>2</sub> by Atomic Doping. Angewandte Chemie - International Edition, 2013, 52, 1664-1667.	13.8	251

#	Article	IF	CITATIONS
145	Electroplated Thick Manganese Oxide Films with Ultrahigh Capacitance. Advanced Energy Materials, 2013, 3, 857-863.	19.5	70
146	Toward the Theoretical Capacitance of RuO <sub>2</sub> Reinforced by Highly Conductive Nanoporous Gold. Advanced Energy Materials, 2013, 3, 851-856.	19.5	184
147	Regulating Infrared Photoresponses in Reduced Graphene Oxide Phototransistors by Defect and Atomic Structure Control. ACS Nano, 2013, 7, 6310-6320.	14.6	112
148	Enhanced catalytic activity in strained chemically exfoliated WS2 nanosheets for hydrogen evolution. Nature Materials, 2013, 12, 850-855.	27.5	2,326
149	Geometrically Controlled Nanoporous PdAu Bimetallic Catalysts with Tunable Pd/Au Ratio for Direct Ethanol Fuel Cells. ACS Catalysis, 2013, 3, 1220-1230.	11.2	152
150	A nanoscale co-precipitation approach for property enhancement of Fe-base alloys. Scientific Reports, 2013, 3, 1327.	3.3	79
151	Structural Features of the Extraordinary Low Glass Transition Temperature for Au <sub>65</sub> Cu <sub>18</sub> Si <sub>17</sub> Bulk Metallic Glass. Materials Transactions, 2013, 54, 1351-1355.	1.2	3
152	Atomic origins of the high catalytic activity of nanoporous gold. Nature Materials, 2012, 11, 775-780.	27.5	803
153	Deposition of multicomponent metallic glass films by single-target magnetron sputtering. Intermetallics, 2012, 21, 105-114.	3.9	52
154	Enhanced mechanical properties of nanocrystalline boron carbide by nanoporosity and interface phases. Nature Communications, 2012, 3, 1052.	12.8	119
155	Characterization of oxide nanoprecipitates in an oxide dispersion strengthened 14YWT steel using aberration-corrected STEM. Acta Materialia, 2012, 60, 5686-5696.	7.9	65
156	Direct synthesis of fullerene-intercalated porous carbon nanofibers by chemical vapor deposition. Carbon, 2012, 50, 5162-5166.	10.3	12
157	Nanoporous Gold Catalyst for Highly Selective Semihydrogenation of Alkynes: Remarkable Effect of Amine Additives. Journal of the American Chemical Society, 2012, 134, 17536-17542.	13.7	201
158	Structural Origins of the Excellent Glass Forming Ability of <mml:math xmlns:mml="http://www.w3.org/1998/Math/MathML" display="inline"&gt;<mml:msub><mml:mi>Pd</mml:mi><mml:mn>40</mml:mn></mml:msub><mml:msub><mml:m mathvariant="normal"&gt;P<mml:mn>20</mml:mn></mml:m </mml:msub>. Physical Review Letters, 2012, 108, 175501.</mml:math 	ni> <b>7\%</b> <td>nl:mis<mml:r< td=""></mml:r<></td>	nl:mis <mml:r< td=""></mml:r<>
159	Coherent Atomic and Electronic Heterostructures of Single-Layer MoS <sub>2</sub> . ACS Nano, 2012, 6, 7311-7317.	14.6	806
160	Thermal properties of nanoporous gold. Physical Review B, 2012, 85, .	3.2	22
161	Tunable Photoluminescence from Graphene Oxide. Angewandte Chemie - International Edition, 2012, 51, 6662-6666.	13.8	584
162	Low temperature uniform plastic deformation of metallic glasses during elastic iteration. Acta Materialia, 2012, 60, 3741-3747.	7.9	30

#	Article	IF	CITATIONS
163	Biofunctionalized nanoporous gold for electrochemical biosensors. Electrochimica Acta, 2012, 67, 1-5.	5.2	60
164	Direct structural evidence for dynamic heterogeneity in supercooled liquid bulk metallic glass. Scripta Materialia, 2012, 66, 927-930.	5.2	7
165	Three-dimensional bicontinuous nanoporous Au/polyaniline hybrid films for high-performance electrochemical supercapacitors. Journal of Power Sources, 2012, 197, 325-329.	7.8	100
166	Innovative processing of high-strength and low-cost ferritic steels strengthened by Y–Ti–O nanoclusters. Materials Science & Engineering A: Structural Materials: Properties, Microstructure and Processing, 2012, 544, 59-69.	5.6	27
167	Tailored nanoporous gold for ultrahigh fluorescence enhancement. Physical Chemistry Chemical Physics, 2011, 13, 3795.	2.8	29
168	Atomic structure of nanoclusters in oxide-dispersion-strengthened steels. Nature Materials, 2011, 10, 922-926.	27.5	306
169	Effect of Residual Silver on Surface-Enhanced Raman Scattering of Dealloyed Nanoporous Gold. Journal of Physical Chemistry C, 2011, 115, 19583-19587.	3.1	66
170	Distorted icosahedral Ni5Nb3Zr5 clusters in the as-quenched and hydrogenated amorphous (Ni0.6Nb0.4)0.65Zr0.35 alloys. Journal of Non-Crystalline Solids, 2011, 357, 3357-3360.	3.1	7
171	Field Emission from Atomically Thin Edges of Reduced Graphene Oxide. ACS Nano, 2011, 5, 4945-4952.	14.6	139
172	Direct observation of local atomic order in a metallic glass. Nature Materials, 2011, 10, 28-33.	27.5	483
173	Nanoporous metal/oxide hybrid electrodes for electrochemical supercapacitors. Nature Nanotechnology, 2011, 6, 232-236.	31.5	1,914
174	Nanoporous gold for enzyme-free electrochemical glucose sensors. Scripta Materialia, 2011, 65, 17-20.	5.2	90
175	Photoluminescence from Chemically Exfoliated MoS <sub>2</sub> . Nano Letters, 2011, 11, 5111-5116.	9.1	3,402
176	Highly optimized embedded-atom-method potentials for fourteen fcc metals. Physical Review B, 2011, 83,	3.2	422
177	Boron effects on the ductility of a nano-cluster-strengthened ferritic steel. Materials Science & Engineering A: Structural Materials: Properties, Microstructure and Processing, 2011, 528, 855-859.	5.6	26
178	Nanoporous PdNi Bimetallic Catalyst with Enhanced Electrocatalytic Performances for Electro-oxidation and Oxygen Reduction Reactions. Advanced Functional Materials, 2011, 21, 4364-4370.	14.9	251
179	Li Storage in 3D Nanoporous Auâ€Supported Nanocrystalline Tin. Advanced Materials, 2011, 23, 2443-2447.	21.0	198
180	Nanoindentation characterization of deformation and failure of aluminum oxynitride. Acta Materialia, 2011, 59, 1671-1679.	7.9	47

#	Article	IF	CITATIONS
181	Nano-twinned structure and photocatalytic properties under visible light for undoped nano-titania synthesised by hydrothermal reaction in water–ethanol mixture. Journal of Supercritical Fluids, 2011, Atomî6and1electronic structure of Pd <mml:math <br="" xmlns:mml="http://www.w3.org/1998/Math/MathML">display="inline"&gt;<mml:msub><mml:mrow< td=""><td>3.2</td><td>22</td></mml:mrow<></mml:msub></mml:math>	3.2	22
182	<pre>aisplay= initie &gt;<mml:mn>40Ni<mml:math display="inline" xmlns:mml="http://www.w3.org/1998/Math/MathML"><mml:msub><mml:mn>40</mml:mn></mml:msub></mml:math>P<mml:math display="inline" xmlns:mml="http://www.w3.org/1998/Math/MathML"><mml:msub></mml:msub></mml:math></mml:mn></pre>	3.2	24
183	Enhanced Electrochemical Performances of Nanoporous Gold by Surface Modification of Titanium Dioxide Nanoparticles. Materials Transactions, 2010, 51, 1566-1569.	1.2	14
184	Addition of Fe2O3 as oxygen carrier for preparation of nanometer-sized oxide strengthened steels. Journal of Nuclear Materials, 2010, 405, 199-202.	2.7	11
185	Correlation between surface whisker growth and interfacial precipitation in aluminum thin films on silicon substrates. Journal of Materials Science, 2010, 45, 3367-3374.	3.7	8
186	A Threeâ€Ðimensional Goldâ€Ðecorated Nanoporous Copper Core–Shell Composite for Electrocatalysis and Nonenzymatic Biosensing. Advanced Functional Materials, 2010, 20, 2279-2285.	14.9	159
187	Influences of grain size and grain boundary segregation on mechanical behavior of nanocrystalline Ni. Materials Science & Engineering A: Structural Materials: Properties, Microstructure and Processing, 2010, 527, 2297-2304.	5.6	55
188	Oxygen reduction in nanoporous metal–ionic liquid composite electrocatalysts. Nature Materials, 2010, 9, 904-907.	27.5	638
189	Effect of doping and counterdoping on high-pressure phase transitions of silicon. Applied Physics Letters, 2010, 96, 251910.	3.3	8
190	Size dependence of molecular fluorescence enhancement of nanoporous gold. Applied Physics Letters, 2010, 96, 073701.	3.3	52
191	On the effect of impurities in metallic glass formation. Applied Physics Letters, 2010, 96, .	3.3	13
192	Deformation-induced change in the structure of metallic glasses during multistep indentation. Physical Review B, 2010, 81, .	3.2	8
193	Coupling between chemical and dynamic heterogeneities in a multicomponent bulk metallic glass. Physical Review B, 2010, 81, .	3.2	74
194	Pressure-induced depolarization and resonance in Raman scattering of single-crystalline boron carbide. Physical Review B, 2010, 81, .	3.2	43
195	Local atomic structure of Ni60Pd20P20 and Ni60Pd20P17B3 bulk metallic glasses and the origin of glass forming ability. Journal of Alloys and Compounds, 2010, 496, 135-139.	5.5	7
196	Electrochemical synthesis of palladium nanostructures with controllable morphology. Nanotechnology, 2010, 21, 085601. Doping and temperature dependence of Raman scattering from cmmkmath	2.6	27
197	xmlns:mml="http://www.w3.org/1998/Math/MathML" display="inline"> <mml:mrow><mml:msub><mml:mrow><mml:mtext>NdFeAsO</mml:mtext></mml:mrow><m xmlns:mml="http://www.w3.org/1998/Math/MathML"</m </mml:msub></mml:mrow>	iml:mrow><	:mml:mn>1<

#	Article	IF	CITATIONS
199	Quantitative electron holographic tomography for a spherical object. Microscopy (Oxford, England), 2009, 58, 301-304.	1.5	1
200	Growth and Nanoscale Magnetic Properties of Ferromagnetic Nanowire Encapsulated Inside Carbon Nanotubes. IEEE Transactions on Magnetics, 2009, 45, 2488-2491.	2.1	3
201	Nanoporous Copper with Tunable Nanoporosity for SERS Applications. Advanced Functional Materials, 2009, 19, 1221-1226.	14.9	336
202	Surface-Enhanced Raman Scattering of Silver@Nanoporous Copper Coreâ^'Shell Composites Synthesized by an In Situ Sacrificial Template Approach. Journal of Physical Chemistry C, 2009, 113, 14195-14199.	3.1	36
203	Formation of an intermediate compound with a B12H12cluster: experimental and theoretical studies on magnesium borohydride Mg(BH4)2. Nanotechnology, 2009, 20, 204013.	2.6	104
204	Microstructural Origin of Superior Compressive Ductility of a Nanocrystalline Metal. Materials Science Forum, 2009, 633-634, 73-84.	0.3	0
205	Characteristic Length and Temperature Dependence of Surface Enhanced Raman Scattering of Nanoporous Gold. Journal of Physical Chemistry C, 2009, 113, 10956-10961.	3.1	79
206	Geometric effect on surface enhanced Raman scattering of nanoporous gold: Improving Raman scattering by tailoring ligament and nanopore ratios. Applied Physics Letters, 2009, 94, .	3.3	75
207	High-pressure Raman spectroscopy of carbon onions and nanocapsules. Applied Physics Letters, 2009, 95, .	3.3	21
208	Atomic-Scale Heterogeneity of a Multicomponent Bulk Metallic Glass with Excellent Glass Forming Ability. Physical Review Letters, 2009, 103, 075502.	7.8	189
209	Doping Effect on High-Pressure Structural Stability of ZnO Nanowires. Journal of Physical Chemistry C, 2009, 113, 1164-1167.	3.1	22
210	Plastic deformation energy of bulk metallic glasses. Materials Science and Engineering B: Solid-State Materials for Advanced Technology, 2008, 148, 101-104.	3.5	19
211	Micromechanisms of serrated flow in a Ni50Pd30P20 bulk metallic glass with a large compression plasticity. Acta Materialia, 2008, 56, 2834-2842.	7.9	75
212	Interface structure and properties of a brass-reinforced Ni59Zr20Ti16Si2Sn3 bulk metallic glass composite. Acta Materialia, 2008, 56, 3077-3087.	7.9	25
213	Characteristic Length Scale of Bicontinuous Nanoporous Structure by Fast Fourier Transform. Japanese Journal of Applied Physics, 2008, 47, 1161.	1.5	80
214	Selected area nanodiffraction fluctuation electron microscopy for studying structural order in amorphous solids. Scripta Materialia, 2008, 58, 303-306.	5.2	10
215	Microstructure and local magnetic induction of segmented and alloyed Pd/Co nanocomposites encapsulated inside vertically aligned multiwalled carbon nanotubes. Diamond and Related Materials, 2008, 17, 1525-1528.	3.9	2
216	Synthesis and Optical Properties of Three-Dimensional Porous Coreâ^'Shell Nanoarchitectures. Langmuir, 2008, 24, 4426-4429.	3.5	40

#	Article	IF	CITATIONS
217	Three-dimensional morphology of nanoporous gold. Applied Physics Letters, 2008, 92, .	3.3	235
218	Unusually Small Electrical Resistance of Three-Dimensional Nanoporous Gold in External Magnetic Fields. Physical Review Letters, 2008, 101, 166601.	7.8	79
219	TEM Sample Preparation for Microcompressed Nanocrystalline Ni. Materials Transactions, 2008, 49, 2091-2095.	1.2	8
220	Electron holography of single-crystal iron nanorods encapsulated in carbon nanotubes. Journal of Applied Physics, 2007, 101, 014323.	2.5	21
221	Electrical conductivity of a bulk metallic glass composite. Applied Physics Letters, 2007, 91, .	3.3	18
222	Encapsulation of segmented Pd–Co nanocomposites into vertically aligned carbon nanotubes by plasma-hydrogen-induced demixing. Applied Physics Letters, 2007, 90, 133116.	3.3	11
223	Ultra-Large Room-Temperature Compressive Plasticity of a Nanocrystalline Metal. Nano Letters, 2007, 7, 2108-2111.	9.1	78
224	Encapsluation of Co and Pd multi-metal nanowires inside multiwalled carbon nanotubes by microwave plasma chemical vapor deposition. Diamond and Related Materials, 2007, 16, 1200-1203.	3.9	15
225	Surface enhanced Raman scattering of nanoporous gold: Smaller pore sizes stronger enhancements. Applied Physics Letters, 2007, 90, 153120.	3.3	333
226	Microstructural characterization of dispersion-strengthened Cu–Ti–Al alloys obtained by reaction milling. Materials Science & Engineering A: Structural Materials: Properties, Microstructure and Processing, 2007, 454-455, 183-193.	5.6	12
227	Quantitative Electron Tomography of Nanoporous Gold. Materia Japan, 2007, 46, 784-784.	0.1	0
228	é›»åç·šãf›ãfã,°ãf©ãf•ã,£ãf¼ã«ãŠãʿã,‹è§£æžæ‰‹æ³•ã@実際. Materia Japan, 2006, 45, 535-539.	0.1	0
229	Application of equal-channel angular pressing to Cu–Co alloy with ferromagnetic precipitates. Materials Science & Engineering A: Structural Materials: Properties, Microstructure and Processing, 2006, 417, 149-157.	5.6	15
230	The aging characteristics of an Al–Ag alloy processed by equal-channel angular pressing. Materials Science & Engineering A: Structural Materials: Properties, Microstructure and Processing, 2006, 437, 240-247.	5.6	37
231	Reconstruction technique for off-axis electron holography using coarse fringes. Ultramicroscopy, 2006, 106, 486-491.	1.9	16
232	Demixing of Solid-Soluted Co-Pd Binary Alloy Induced by Microwave Plasma Hydrogen Irradiation Technique. Japanese Journal of Applied Physics, 2006, 45, L860-L863.	1.5	5
233	Cobalt nanorods fully encapsulated in carbon nanotube and magnetization measurements by off-axis electron holography. Applied Physics Letters, 2006, 88, 243118.	3.3	19
234	Precipitation Behavior in Age-Hardenable Alloys after Severe Plastic Deformation. , 2006, , 129-136.		0

#	Article	IF	CITATIONS
235	Grain refinement and superplastic flow in an aluminum alloy processed by high-pressure torsion. Materials Science & Engineering A: Structural Materials: Properties, Microstructure and Processing, 2005, 408, 141-146.	5.6	84
236	Phase recovery for electron holography using Gerchberg–Papoulis iterative algorithm. Ultramicroscopy, 2005, 102, 279-286.	1.9	6
237	Achieving High Strength and High Ductility in Precipitation-Hardened Alloys. Advanced Materials, 2005, 17, 1599-1602.	21.0	273
238	Microstructures after Processing by Aging and ECAP for Al-Mg <sub>2</sub> Si Alloys Containing Excess Si or Mg. Materials Science Forum, 2005, 475-479, 4047-4050.	0.3	2
239	Crystallographic orientation contrast associated with Ga+ ion channelling for Fe and Cu in focused ion beam method. Journal of Electron Microscopy, 2004, 53, 571-576.	0.9	19
240	Determination of absolute thickness and mean free path of thin foil specimen by Â-factor method. Journal of Electron Microscopy, 2004, 53, 137-142.	0.9	7
241	Using grain boundary engineering to evaluate the diffusion characteristics in ultrafine-grained Al–Mg and Al–Zn alloys. Materials Science & Engineering A: Structural Materials: Properties, Microstructure and Processing, 2004, 371, 241-250.	5.6	79
242	Microstructural Control of a Precipitate-Hardenable Al-Ag Alloy Using Severe Plastic Deformation. Materials Science Forum, 2003, 426-432, 2637-2642.	0.3	9
243	Diffusion Analysis across Grain Boundary in Al-3.7 mass%Cu Alloy Using Analytical Electron Microscopy. Materials Transactions, 2003, 44, 1336-1342.	1.2	0
244	Relationship between Misorientation Angle and Precipitate Free Zones of Warm Rolled 7475 Based Aluminum Alloy Sheet. Materia Japan, 2003, 42, 857-857.	0.1	0
245	Deformation of Second Phase Particles in Al Alloy Using Severe Plastic Deformation Process. Materia Japan, 2003, 42, 863-863.	0.1	2
246	Characteristics of diffusion in Al-Mg alloys with ultrafine grain sizes. Philosophical Magazine A: Physics of Condensed Matter, Structure, Defects and Mechanical Properties, 2002, 82, 2249-2262.	0.6	73
247	Diffusion in Fine-Grained Al Alloys Having Low and High Angle Grain Boundaries. Materials Science Forum, 2002, 396-402, 1061-1066.	0.3	5
248	Construction of Ti-Al-Cr Phase Diagram Using Quantitative X-ray Microanalysis in Analytical Electron Microscope. Nippon Kinzoku Gakkaishi/Journal of the Japan Institute of Metals, 2001, 65, 382-388.	0.4	8
249	SIM Observation of Ultrafine-Grained Al Alloy After Superplastic Deformation. Materia Japan, 2000, 39, 984-984.	0.1	0
250	Advanced form of Â-factor method in analytical electron microscopy. Journal of Electron Microscopy, 1999, 48, 561-568.	0.9	2
251	Conversion of methane with carbon dioxide into C2 hydrocarbons over metal oxides. Applied Catalysis A: General, 1995, 126, 245-255.	4.3	60
252	Determination of Technetium by Laser Induced Photoacoustic Spectroscopy Coupled with a Wave-Length Shifter Method. Radiochimica Acta, 1993, 63, 45-48.	1.2	4